Title: Modulating Protein-Protein Interactions with Visible-Light Responsive Peptide Backbone Photoswitches

Authors: Lea Albert; Alberto Peñalver; Nemanja Djokovic; Laura Werel; Malte Hoffarth; Dusan Ruzic; Jing Xu; Lars-Oliver Essen; Katarina Nikolic; Yali Dou; Olalla Vazquez

To be cited as: ChemBioChem 10.1002/cbic.201800737

Link to VoR: https://doi.org/10.1002/cbic.201800737

Modulating Protein-Protein Interactions with Visible-Light Responsive Peptide Backbone Photoswitches

Lea Albert,[a] Alberto Peñalver,[a] Nemanja Djokovic,[b] Laura Werel,[a] Malte Hoffarth,[a] Dusan Ruzic,[b] Jing Xu[c], Lars-Oliver Essen,[a] Katarina Nikolic,[b] Yali Dou,[c] Olalla Vázquez*[a]

Abstract: Life relies on a myriad of carefully orchestrated processes, in which proteins and their direct interplay ultimately determine cellular function and disease. Modulation of these complex cross-talks has recently attracted attention, even as a novel therapeutic strategy. Here, we describe the synthesis and characterization of two visible-light responsive peptide backbone photoswitches based on azobenzene derivatives to exert optical control over protein-protein interactions (PPI). Our novel peptidomimetics undergo fast isomerization and reversibility with low photochemical fatigue under alternatively blue/green-light irradiation cycles. Both bind in the nanomolar rage to the protein of interest. Importantly, our best peptidomimetic displays a clear difference between isomers in its protein-binding capacity and, in turn, in its potential to inhibit enzymatic activity via PPI disruption. In addition, crystal structure determination, docking and MD calculations give a molecular interpretation and open new avenues in the design and synthesis of future photoswitchable PPI modulators.

Introduction

Proteins play a key role in the regulation of cellular behavior and are, therefore, also involved in the development of diseases. Despite the fact that some proteins perform their functions independently, the reality is that most of them are integrated in complex dynamic networks ruled by protein-protein interactions (PPIs).[1] These cross-talks control both protein production and activity as well as signal transduction and metabolic pathways. Therefore, breaking the molecular code associated with PPIs will pave the way for on-demand modulation of functional outcomes capable of affecting pathogenic mechanisms. Historically, PPIs with relatively large buried interfaces have been considered 'undruggable' targets.[2] However, the last years have witnessed an outstanding success in targeting PPIs by many different approaches such as: small-molecule derivatives, recombinant proteins, antibodies, and peptides.[3] In particular, the use of peptidomimetics has acquired more and more relevance because they not only retain the advantages of peptides but also overcome their intrinsic limitations providing new features.[4] For example, by grafting a light-driven molecular transducer onto a peptide scaffold, space-temporal resolution could be achievable to circumvent the common off-target effects in therapy.

Azobenzenes[5] are by far the most extensively used photoswitches in the context of photopharmacology.[6] However, their *trans* → *cis* isomerization wavelengths at 366 nm is not the ideal one for in vivo applications and, furthermore, this photoisomerization is not complete neither. Therefore, in the last few years there has been a great interest in developing visible-light-shifting azobenzenes to overcome such limitations.[7] Among these second-generation compounds, the cyclic azobenzene 5,6-dihydrodibenzo[c,g][1,2] diazocine is a very interesting one.[8] Thus, the C2 bridge produces a highly twisted *trans* isomer that is less stable than the *cis* conformation—the opposite situation to 'normal' azobenzenes. *p*-Acetoamido substituents in the cyclic azobenzene core enable slightly red-shifted isomerization wavelengths.[9] More importantly, the separation of the n→π* transition is large (85 nm) so that selective irradiation is possible. The same behavior was also observed with tetra-*ortho*-substituted azobenzenes.[10] In particular, the group of Hecht has currently optimized the properties of the classical azobenzenes by introducing σ-electron-withdrawing fluorine atoms in these positions, which leads to visible-light switches with high photoconversions and very long-lived *cis* isomers.[7c] Since Hecht's contribution, tetra-*ortho*-fluoroazobenzenes have been mainly used in material science[11] and their applications in biological context are scarce.[12] Along these lines, there have been only a few cyclic azobenzene derivatives used to modulate DNA hybridization[13] and to control the helical conformation of peptides.[9b]

Regarding azo-containing proteins and peptides, the strategies employed to introduce red-shifted azobenzenes are mainly restricted to cysteine-reactive tethered derivatives as side-chain crosslinkers[14] and genetic encoding of the azobenzene amino acids.[15] However, to the best of our knowledge, the direct inclusion of the azobenzene unit into peptide backbones is still limited to the unsubstituted derivatives as the classic Fmoc-building blocks: [3-(3-amino-methyl)phenylazo]phenylacetic acid (AMPP),[16] (4-aminomethyl)phenylazobenzoic acid (AMPB),[17] and the commercial Fmoc-L-phenylalanine-4'-azobenzene.

Herein, we describe the synthesis and characterization of two novel visible-light photocontrollable amino acids based on the on the previous scaffolds of Bléger et al.[18] and Siewertsen et al.[8] in

[a] L. Albert, A. Peñalver, L. Werel, M. Hoffarth, Prof. Dr. L.-O. Essen and Jun.-Prof. Dr. O. Vázquez
Fachbereich Chemie
Philipps-Universität Marburg
Hans-Meerwein-Straße 4, 35043, Marburg, Germany
E-mail: olalla.vazquez@staff.uni-marburg.de
[b] N. Djokovic, D. Ruzic and K. Nikolić
Department of Pharmaceutical Chemistry, Faculty of Pharmacy
University of Belgrade
450 Vojvode Stepe Street, Belgrade, Serbia
[c] Dr. J. Xu, Prof. Dr. Y. Dou
Department of Pathology
University of Michigan
Ann Arbor, Michigan 48109, USA

Supporting information for this article is given via a link at the end of the document.

order to be grafted onto a peptide scaffold. Since our group has recently reported the possibility of externally controlling leukemia cell proliferation by disrupting the essential epigenetic PPI: MLL1-WDR5 with photoswitchable azobenzene-containing peptides,[19] we will use this biological system to study the potential as novel PPI modulators. So far, to the best of our knowledge, no attempts incorporating either the tetra-*ortho*-fluoroazobenzenes or cyclic derivatives into peptide backbones have been reported. Exploring second-generation azobenzenes as visible-light responsive peptide backbone photoswitches will complement the information to those, where the photoswitches are attached to the N-terminus of the peptide sequence, or on the side chain of an amino acid as crosslinkers. Furthermore, it will contribute to gain an insight into peptidomimetics design.

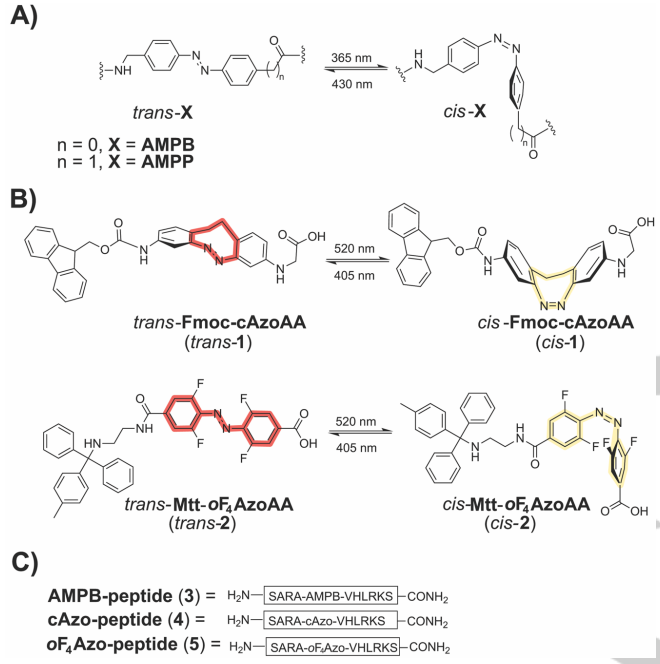

Figure 1. A) Previously reported light-responsive peptide backbone photoswitches. B) Structure and isomerization of the new visible-light photoswitchable amino acids reported here: **Fmoc-cAzoAA** (**1**) and **Mtt-*o*F4AzoAA** (**2**). C) Former photoswitchable peptidomimetic used for MLL1-WDR5 PPI disruption (**3**) and the new ones, which contain the visible-light responsive peptide backbone photoswitches.

Results and Discussion

Synthesis of the Photoswitchable Building Blocks and Inclusion into Peptide Backbone

To simplify the synthetic work even at the expense of moderate yields, we followed the previous procedures of azobenzene cyclization[9] and obtained the compound **6**. Afterwards, one of the primary amines was mono-alkylated while the remaining one was protected with Fmoc-chloride. The final hydrolysis step yielded the corresponding **Fmoc-cAzo AA** (**1**).

The synthesis of peptide backbone switches would be more accessible if our molecular transducers were compatible with Fmoc solid-phase peptide synthesis (Fmoc-SPPS). However, the presence of halide substituents in the azobenzene derivatives turns them susceptible of aromatic nucleophilic substitutions (S_NAr) under the conventional Fmoc-deprotection conditions (i.e. 20% piperidine/DMF).[20] Consequently, we envisioned using the 4-methyl trityl (Mtt) group[21] as acid-labile amine protecting group because it is fully orthogonal to the side-chain ones. Thus, the symmetric di-carboxylic tetra-*ortho*-fluorazobenzene (**9**),[18] was mono-functionalized at the *para* position by the condensation with the previous synthesized Mtt-protected ethylendiamine[22] under standard amidation conditions. This reaction provided the **Mtt-oF4AzoAA** (**2**) compound in moderate yields.

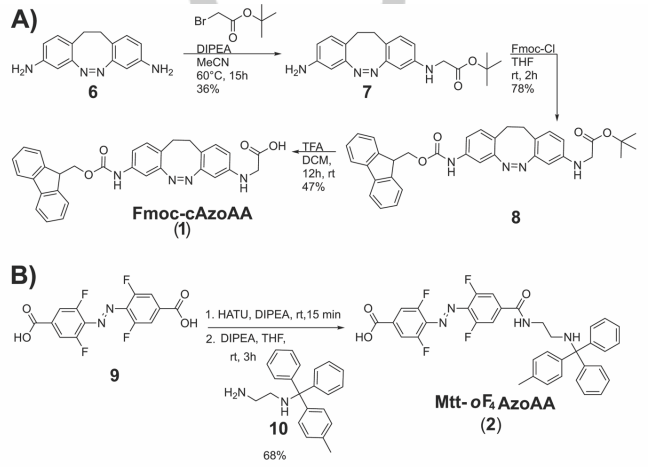

Scheme 1. Synthetic routes of the visible-light photoswitchable amino acids. A) **Fmoc-cAzoAA** (**1**). B) **Mtt-oF4AzoAA** (**2**).

Once the newly synthesized photoswitchable building blocks were characterized with regard to their purity and structural integrity (see Supporting Information for details), they were incorporated into the peptide backbone of our previous PPI modulator **3**, replacing the AMPB group. The synthesis of the **cAzo-peptide** (**4**), which bears the cyclic azobenzene derivative was straightforward. On the contrary, the extension of the peptide chain after **Mtt-oF4AzoAA** inclusion required optimization. Thus, we explored mild deprotection methods for achieving the efficient removal of the Fmoc group without affecting the integrity of the molecular transducer. As shown in Table 1, the use of few weaker but more sterically hindered bases than piperidine (pKa 11.12)[23] such as the tertiary amines: *N*, *N*'-diisopropylethylamine (DIPEA, pKa 10.75), triethylamine (Et_3N, pKa 10.78) and tributylamine (Bu_3N, pKa 10.89) caused prolonged reaction times, incomplete conversion and also detectable chemical degradation (Figures S11 & S12). Instead, complete deprotection was accomplished with a 20 mM solution of sodium hydroxide in 30% dioxane/MeOH after only 30 min.[24] Unfortunately, the reaction did not only yield the desired product but also substitution side products (Figure S12 Right). Likewise, other alternative conditions like piperazine and 1,8-diazabicyclo[5.4.0]undec-7-ene (DBU) treatment were previously discharged due to the detection of substitution side products with **9** (Figure S9). Only a solution of potassium fluoride (6.5 eq) in DMF with catalytic amounts of 18-crown-6 provided the

deprotection product neatly (Figure S13).[24] However, due to time reasons we resorted to peptide synthesis in solution via chemical ligation (see Supporting Information for details) to obtain the peptidomimetic **5** bearing the tetra-*ortho*-fluoroazobenzene derivative (***o*F$_4$Azo-peptide**).

Table 1. Tested conditions for mild Fmoc-deprotection of a tetra-*ortho*-fluoroazobenzene-containing peptide on solid support at 25 °C.

	Conditions	Time/h	Product	Starting Material	Side Products
A	50% Et_3N in CH_2Cl_2	17	✓	✓	✓
B	50% Bu_3N in CH_2Cl_2	17	✓	✓	✓
C	50% DIPEA in CH_2Cl_2	17	✓	✓	✓
D	20 mM NaOH in 30% dioxane/ methanol	1.5	✓	×	✓
E	KF, 18-crown-6 in DMF	3	✓	✓	×
F	KF, 18-crown-6 in DMF	16	✓	×	×

Photochemical Behavior of the Photoswitchable Peptidomimetics

The isomerization of the photoswitchable peptidomimetics **4** and **5** in aqueous solution was studied by UV-visible spectroscopy, HPLC and NMR. A 0.128 mM solution of the **cAzo-peptide** (**4**) prepared in the dark exhibited bands at λ_{max} = 295 nm and 402 nm for the π→π* and n→π* transitions, respectively. This is consistent with the photochemical behavior of the *cis* unsubstituted parental cyclic azobenze.[8] Irradiation with a blue-light LED (405 nm, see Supporting Information for details) lead to spectroscopic changes in the solution: an increase of a band at λ_{max} = 475 nm. Thus, in the photostationary state (PSS) at 405 nm the n→π* transition is shifted to longer wavelengths. The PSS was reached after just one second of irradiation (Figure S16). Importantly, there is a spectral region (500–550 nm) where essentially only this isomer absorbs, which consequently enables quantitative *cis* isomerization under green-light LED irradiation (520 nm, see Supporting Information for details). Additional spectral changes were detected in the region of the π→π* (λ_{max} = 295 nm), where the absorption of the PSS at 405 nm was stronger than the PSS at 520 nm. Unlike the *trans* unsubstituted parental cyclic azobenze[8] as well as the *trans* 4,4' and 3,3' *p*-acetamido-substituted ones,[9] no decrease of the band at λ_{max} 402 nm was observed in the **cAzo-peptide** (**4**), what was also observed in the 3,3' polyurea-substituted analogues.[25] Upon irradiation with the green light the spectrum reverted to the one of the thermodynamically favored *cis* isomer. In case of the ***o*F$_4$Azo-peptide** (**5**), the *trans* isomer is the most stable thermodynamically. Thus, a 0.105 mM solution of **5** prepared in the dark exhibited the characteristic absorption bands of the *trans* tetra-*ortho*-fluoroazobenze isomers:[7c] intense band at λ_{max} = 319 nm and a weaker one at λ_{max} = 457 nm assigned to the π→π* and n→π* transitions, respectively. After 30 seconds of continuous irradiation with the green-light LED the *cis* photostationary state was reached (Figure S15), which lead to a drastic decrease of the band at λ_{max} = 319 nm, a shift of the weaker band to shorter wavelengths (λ_{max} = 412 nm) and an increase of a band at λ_{max} = 250 nm. Irradiation at 405 nm reverted the spectrum to that of the *trans* isomer.

We next monitored the UV-vis absorptions of the aqueous solutions of **4** and **5** after alternating irradiation cycles at 405 nm and 520 nm. We demonstrated the reversibility of the photo-isomerization (up to ≥ 14 cycles) for our peptide backbone photoswitches without any signs of photodegradation and photo-chemical fatigue (Figure 2 B).

For the determination of both the ratio and the stability of the isomers in the photostationary state, we used HPLC chromatography. In case of the ***o*F$_4$Azo-peptide** (**5**), we integrated the peak area of the different chromatograms at the

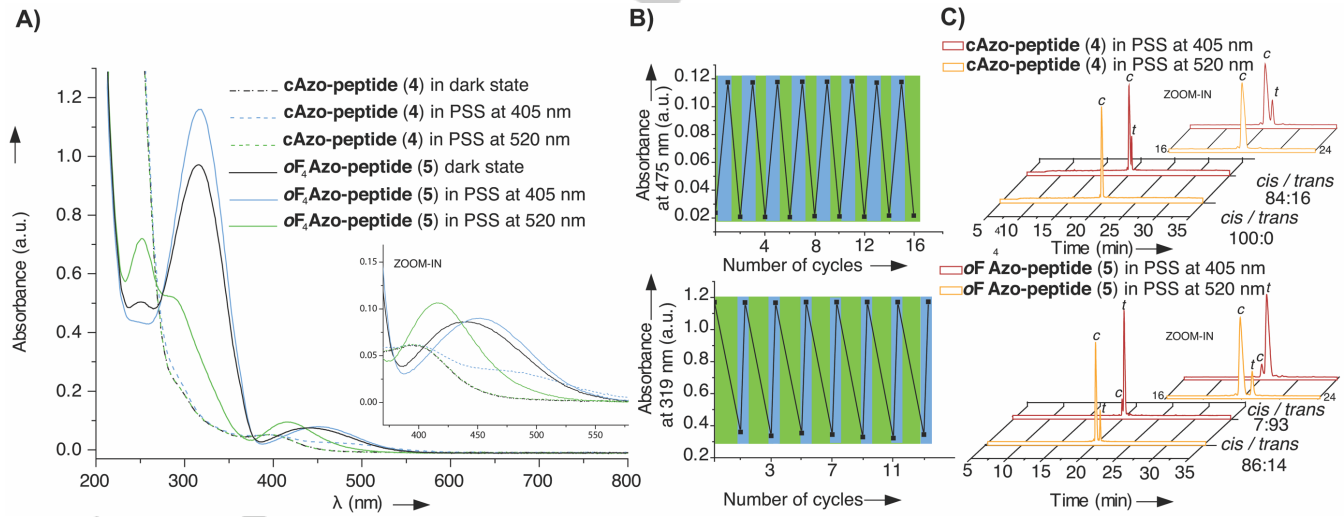

Figure 2. A) UV-vis spectra of aqueous solutions of the peptidomimetics **4** (0.128 mM; dashed lines) or **5** (0.105 mM; straight lines) in the photostationaty states (PSS) at 405 nm (blue) and 520 nm (green) at 25 °C. Insert displays a zoom in the 350-600 nm region of the spectra. B) Reversible photochroism of **4** (top) and **5** (bottom) at 475 nm and 319 nm, respectively, upon alternating intervals of irradiation at 405 nm (blue) or 520 nm (green) irradiation at 25 °C. C) HPLC chromatograms and isomer ratio in the PSS at 405 nm (red) and 520 nm (orange) of **4** (top) and **5** (bottom) at 25 °C. Inserts display zoom in 16-24 min region.

isosbestic point (275 nm) and corroborated isomer-conversion ratio by ^{1}H-NMR (Figure S19); for the **cAzo-peptide** (**4**), the HPLC chromatograms were recorded at 395 nm since both isomers exhibited the same intensity in absorption and, therefore, the same extinction coefficient. There was no clear isosbestic point. In both cases the photoconversions were efficient with ratios over 85% for the corresponding isomers (Figure 2 C) except for the isomerization of the peptidomimetic **4** upon blue-light LEDs, where just 16% of the *trans* isomer was detected at the photostationary state. This rather low conversion rate could be attributed to the overlap of the π→π* and n→π* transitions in the *cis* isomer.[9a, 25]

Regarding the thermal stability, at room temperature the isomer ratios at the photostationary states are constant for at least 24 hours in all the cases as long as the solutions are stored in total darkness (Figures S17 & S18). After four days, there is no dramatic change in the isomer distribution, but side products were detected (< 8% in the PSS at 520 nm of both compounds and in PSS at 405 nm of **5**; Figures S17 & S18). Interestingly, this degradation is more pronounced when the cyclic azobenzene-containing peptide (**cAzo-peptide**, **4**) is in the photostationary state at 405 nm (*cis*/*trans* 84:16). There, the detected side products amounted 29% and the substrate further degraded to 50% after one week (Figure S18). Nevertheless, stabilities up to three days are compatible with the vast majority of biological assays.

Certain azobenzene derivatives are susceptible to reduction by intracellular thiols, while others are not. Glutathione (GSH) is the primary intracellular reducing agent, whose expected highest intracellular concentration is 10 mM.[26] In order to have the possibility to use our compounds in a biological context, we evaluated the stability of both **cAzo-peptide** (**4**) and ***o*F$_4$Azo-peptide** (**5**) in presence of 10 mM of glutathione. Interestingly, the behavior of the peptidomimetics is different: while the ***o*F$_4$Azo-peptide** (**5**) was completely resistant to GSH reduction in both PSSs for four days (Figure S20) the **cAzo-peptide** (**4**) was found to be sensitive after just one day (Figure S21). This degradation effect was more severe in the PSS at 405 nm, which is in agreement with our previous stability tests.

Binding Affinity of the Photoswitchable Peptidomimetics to WDR5 and Inhibition of MLL1 Activity

In our previous project we demonstrated that the AMPB-containing peptide (**AMPB-peptide**, **3**) is able to efficiently inhibit MLL1 activity via strong binding to the protein WDR5 (K_i in low nM range for both isomers).[19] WDR5 belongs to the MLL1 protein core complex and is essential as WDR5 knockdown totally abolishes the histone methyltransferase (HMT) function of MLL1.[27] The newly synthetized peptidomimetics **4** and **5** are analogues to the **AMPB-peptide** (**3**) bearing either the cyclic azobenzene derivative or the tetra-*ortho*-fluoroazobenzenze, respectively. Thus, once these visible-light photoswitchable peptidomimetics were synthesized and photochemically characterized, we investigated their WDR5-binding capacities and the possible differences between isomers. To this end, we used our previous optimized fluorescence polarization (FP) competitive assay[19] exchanging only the irradiation step. We included the corresponding controls to rule out any interference with the isomerization (see Supporting Information for details; Figures S22-25). The obtained results are summarized in Figure 3 and in Tables 2, where the IC_{50} values (Table S1) were transformed into the inhibition constant ones (K_i) to enable objective comparisons,[28] in particular, with our former **AMPB-peptide** (**3**).

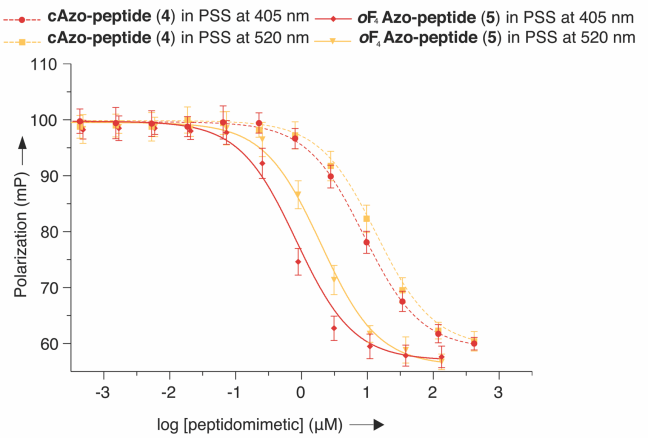

Figure 3. Fluorescence polarization (FP)-based competitive assays of the peptidomimetics: **4** (dashed lines) and **5** (straight lines) in the photostationary state (PSS) at: 405 nm (red); circles and diamonds, respectively, and 520 nm (orange); squares and triangles, respectively at 25 °C. Mean data-points and standard deviations are derived from three independent experiments.

All our novel peptidomimetics interacted with WDR5 with high affinity, in the nanomolar range (Table 2). In comparison with our previous results, the **AMPB-peptide** (**3**), proved to be the photoswitchable peptidomimetic with the highest affinity to WDR5 as well as the biggest difference between isomers (K_i = 1.25 nM for *trans* **3**; K_i = 6.50 nM for *cis* **3**; ratio: 5.0). Thus, the exchange of the azobenzene by the cyclic analogue caused a more than 100-fold decrease in the affinity to WDR5 compared with the **AMPB-peptide** (**3**) while, as expected, the incorporation of the small fluorine atoms into the azobenzene unit (***o*F$_4$Azo-peptide**, **5**) affected the binding properties just slightly. Furthermore, the improved photoconversion properties of the ***o*F$_4$Azo-peptide** (**5**) were not directly translated into higher differences between isomers in our FP-binding assays compared with the **AMPB-peptide** (**3**). Nevertheless, it should be remembered that even low photoconversions can trigger significant biological effects. Taken together all our results so far, we selected the ***o*F$_4$Azo-peptide** (**5**) for further biological assays.

Table 2. Binding affinities of the photoswitchable peptidomimetics to WDR5 at 25 °C

Peptidomimetic	PSS at 405 nm K_i / [nM]	PSS at 520nm K_i / [nM]	Ratio
cAzo-peptide (**4**)	140 ± 35	207 ± 52	1.5
***o*F$_4$Azo-peptide** (**5**)	11.8 ± 1.4	30.8 ± 3.3	2.6

Next we explored if the visible-light photoswitchable peptidomimetic **5** can modulate the essential PPI of the MLL1 core complex (MLL1-WDR5) and, in turn, MLL1 activity. To this end and to avoid radioactivity, we used an amplified luminescent proximity homogeneous (AlphaLISA)- assay[29] with the 4-mer reconstituted MLL1 core complex (i.e. MLL1, WDR5, RbBP5, and Ash2L), the H3-21mer peptide as substrate and the cofactor S-adenosyl methionine (SAM) as universal methyl group donor. Gratifyingly, the functional data obtained from our AlphaLISA-based MLL HMT assay demonstrated that the ***o*F$_4$Azo-peptide** (**5**) effectively inhibited MLL1 activity (Figure 4; IC_{50} for *trans* **5** = 0.927 ± 0.034 µM, IC_{50} for *cis* **5** = 1.73 ± 0.12 µM) via the disruption of the WDR5-MLL1 PPI due to its high affinity to WDR5. Of note, these determined potencies are based on the ability of the ***o*F$_4$Azo-peptide** (**5**) to inhibit the mono- and dimethylation function of the reconstituted MLL1 core complex. In addition, we could observe a modest, yet clear, difference between isomers up to 1.8-fold. To further corroborate the effective PPI disruption by ***o*F$_4$Azo-peptide** (**5**) and the slight difference between isomers, we performed gluthathione-sepharose-transferase (GST) pull-down experiments. We incubated 0.262 µM GST-tagged MLL1 protein with the remaining proteins of the core complex to a final concentration of 0.4 µM. Afterwards, increasing amounts of the ***o*F$_4$Azo-peptide** isomers were added. Both isomers were able to disrupt the MLL1 complex in a dose-dependent fashion. Importantly we demonstrated different behaviors between isomers, where the *trans* isomer, again, showed higher dissociation potential via its higher affinity to WDR5. These results are consistent with our FP-based experiments as well as with the AlphaLISA-based MLL HMT assays. Therefore, collectively our results confirm that visible-light irradiation triggers conformational changes in the peptidomimetic **5**, which affect its capacity to modulate the WDR5-MLL1 PPI and, consequently, its potential to inhibit MLL1.

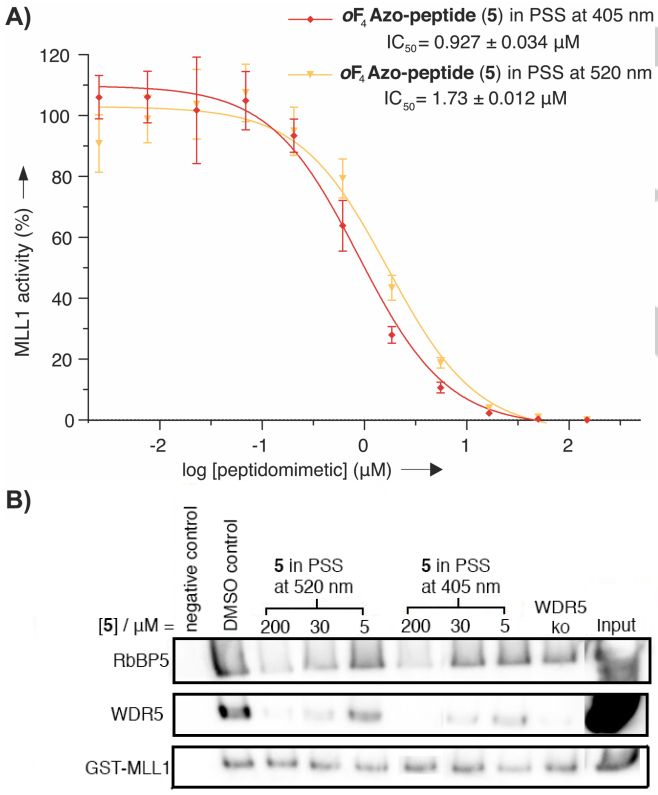

Figure 4. A) In vitro functional HMT AlphaLISA assay to evaluate the potency of the peptidomimetic **5** to inhibit MLL1 enzymatic activity in the photostationary state (PSS) at 405 nm (red, diamonds) and 520 nm (orange, triangles). Mean data-points and standard deviations are derived from three independent experiments. B) In vitro GST- pull down assay with the reconstituted 4mer MLL1 core complex in presence of **5** in the photostationary state (PSS) at 405 nm and 520 nm; ko = knockout.

Crystal Structure Determination and Structural Bases of the Peptidomimetic-WDR5 Interaction

To understand the molecular principles behind the observed affinity deviations, we aimed at crystallizing WDR5 in complex with the peptidomimetics **4** and **5**. No crystals were obtained for ***o*F$_4$Azo-peptide** (**5**) in any PSSs, as of yet. Co-crystallization with **cAzo-peptide** (**4**) in the PSS at 520 nm (*cis* isomer) yielded crystals diffracting to 1.51 Å resolution (PDB code: 6IAM).

Table 3. Data collection and refinement of the co-crystal structure of WDR5 in complex with **cAzo-peptide** (**4**). (PDB code 6IAM).

Data collection	Values
Wavelength (Å)	0.873 Å
Resolution range (Å)	37.49 - 1.51 (1.564 - 1.51)
Space group	P 1 21 1
Unit cell (Å,°)	a = 46.53, b = 46.56, c = 66.17, α = 90, β = 107, γ = 90
Total reflections	167527 (15726)
Unique reflections	42377 (4073)
Multiplicity	4.0 (3.9)
Completeness (%)	99.3 (96.2)
Mean I/σ(I)	9.04 (1.50)
Wilson B-factor (Å^2)	11.27
R_{merge} (%)	0.0899 (0.713)
Refinement statistics	
R_{work}/ R_{free} (%)	0.148/ 0.181
Number of atoms	2895
Protein	2377
Ligands	100
Solvent	418
Protein residues	322
RMS(bonds/angles) (Å/°)	0.009/ 1.08
Ramachandran favored (%)	96.15

Ramachandran outliers (%)	0.00
Rotamer outliers (%)	0.36
Clashscore	2.20
Average B-factor (Å^2)	16.1
PDB code	6IAM

The complex of WDR5 with the **cAzo-peptide** (**4**) appears in a monoclinic crystal form (Table 3) that is distinct from previous crystal packings observed for WDR5-peptide complexes; most likely due to packing of the cyclic azobenzene moiety against Pro168 of a symmetry-related complex. Nevertheless, the WDR5 structure is almost unaffected with a low rmsd of 0.200 Å for 262 Cα atoms when superimposed on the WDR5-histone 3 peptide complex (PDB code: 2CO0).[30] The peptide-bound WDR5 adopts the well-established β-propeller conformation with a central cavity that accommodates the Arg3 side chain[31] that is part of the N-terminal recognition motif of the **cAzo-peptide** (**4**). The superimposition of the **cAzo-** (**4**) and **AMPB-peptide** (**3**) (Figure 5B) reveals almost identical interactions of the N-terminal stretches (SARA) with WDR5 including bridging water molecules and an α-helical main chain trace. However, the central cyclic azobenzene (cAzo) moiety packs differently to WDR5 than the linear azobenzene group of the **AMPB-peptide** (**3**). For example, the cAzo group lacks any direct interactions with the side chains of Lys259 and Tyr260, which are otherwise found for the WDR5-**AMBP-peptide** (**3**) complex. The C-terminal stretch of the **cAzo-peptide** (**4**) (Val6-Ser11) is fully ordered, maybe due to interaction of the C-terminal carboxamide group with a symmetry-related WDR5 molecule, and adopts an α-helical conformation not observed before for any cocrystals between WDR5 and MLL-derived peptides (Figure S26 Right). Apart from additional packing interactions, the **cAzo-peptide** (**4**) establishes here three water-mediated hydrogen bonds: the side-chain carbonyl group of Asp172 interacts with the backbone carbonyl group of Arg9 from the ligand. Likewise, the side-chain hydroxyl group of Tyr191 as well as the amino group of the Lys259 coordinate a water molecule that bridges to the C-terminal backbone carbonyl of the cAzo entity (Figures S27 & S28).

We reported **AMPB-peptide** (**3**) to have an increased affinity in comparison to the WIN peptide (PDB code: 3EG6) in a previous publication.[19] As the **cAzo-peptide** (**4**) lacks quite a few of peptide's **3** interactions, it comes as no surprise that it has a lower binding affinity, which is, indeed, more comparable to the WIN peptide than to the **AMPB-peptide** (**3**) (K_i = 120 nM for WIN peptide; K_i = 140 nM for *cis* **4** and K_i = 1.25 nM for *trans* **3**)

Molecular Modeling of Peptidomimetics-WDR5 Interaction

In order to further rationalize the obtained experimental results and to set up a workflow for further design of novel photoswitchable peptidomimetics, series of virtual docking (VD) and molecular dynamics (MD) calculations were performed.

For all six ligands: *cis/trans* **AMPB-peptide** (**3**), *cis/trans* **cAzo-peptide** (**4**), *cis/trans* **oF$_4$Azo-peptide** (**5**), initial poses for MD calculations were obtained by molecular docking. The docking protocol was validated with heavy atoms RMSD = 0.8915 calculated for the part of the *trans* **AMPB-peptide** (**3**) already resolved in the crystal structure (PDB code: 5M23; Figure S29).[19] Considering the significant conformational flexibility of peptidomimetics, several initial protein-ligand complexes for each ligand were generated. Only protein-ligand complexes, in which the N-terminal part of peptidomimetics (SARA-) remained stabilized during 20 ns MD production runs were used for further analysis. Results of MD simulations expressed as root-mean-squared deviations (RMSD) fluctuations of the N-terminal part of peptidomimetics (SARA-) (Figure 6), and the whole protein (Figure S30) during 20 ns of production runs indicate reasonably stabilized complexes converged to the equilibration state.

The Molecular Mechanics Poisson-Boltzmann Surface Area (MM/PBSA) calculations of the binding energy were performed on the last 7 ns of each simulation in order to further validate predic-

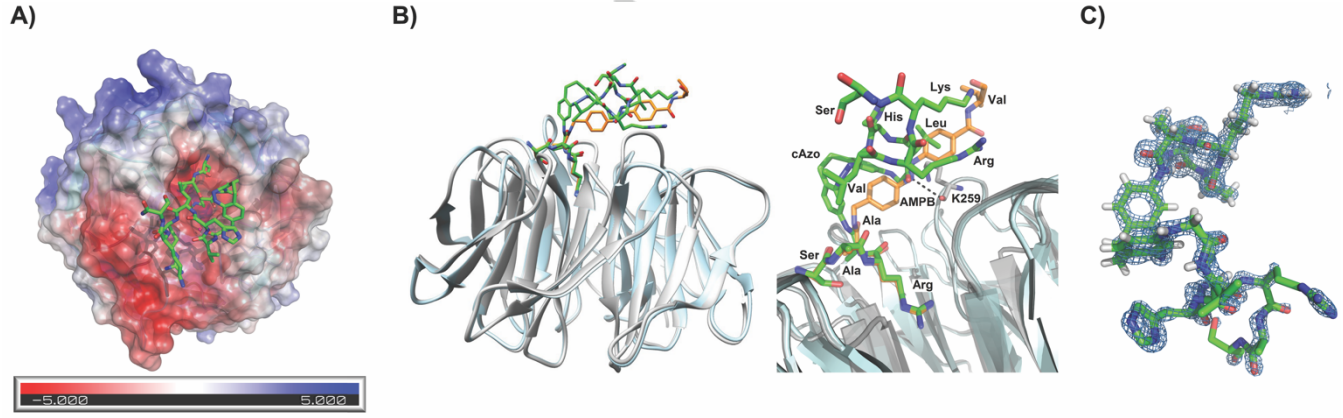

Figure 5. A) Crystal structure of WDR5 in complex with the **cAzo-peptide** (**4**) (PDB code: 6IAM), WDR5 is shown as surface representation of its electrostatic potential with the color code from red (negative) to blue (positive) in dimensionless units of kb. T/ ec, where kb is Boltzmann's constant, T is the temperature, and ec is the charge of an electron (generated using the APBS Pymol plug-in). B) Left: side view of the superimposed co-crystal structures of **AMPB-** (**3**) (orange) and **cAzo-peptide** (**4**) (green) to WDR5. Right: Close-up view of the left overlay, the key hydrogen between **AMPB-peptide** (**3**) and WDR5 (K259) is highlighted; labelling residues and azobenzene motives. C) 2Fo—˜Fc Experimental electron density map contoured at 1.0 sigma (blue) shows the density for **cAzo-peptide** (**4**).

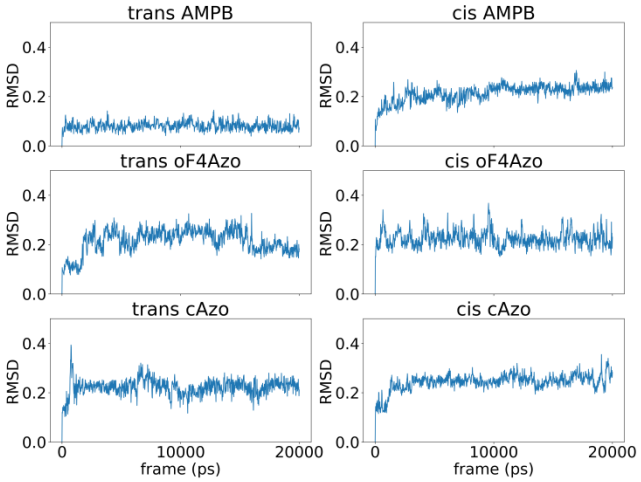

Figure 6. RMSD fluctuations during 20 ns of molecular dynamics production runs calculated for SARA- sequence of the ligands.

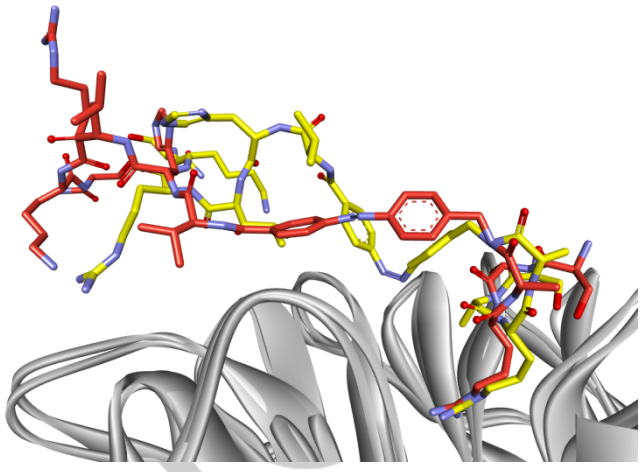

Figure 7. Difference in the binding modes obtained for the *trans* **AMPB-peptide** (**3**) (red) and the *cis* **AMPB-peptide** (**3**) (yellow) inside of WDR5 binding site.

ted binding modes of the peptidomimetics and to investigate a relationship between experimental K_i values (transformed in $pK_{i\,exp}$=-$logK_i$) derived for the synthesized photoswitchable peptidomimetics and their calculated MM/PBSA scores. A linear regression model with R^2=0.88 between aforementioned parameters was established (Table 4), indicating that this model could be used as a predictive tool with discriminative properties between *cis* and *trans* isomers for structurally similar peptidomimetics.

In order to gain insight into details of the molecular interactions, after trajectory clustering procedure, obtained cluster representatives were further analyzed. For all of the examined ligands, the largest fluctuations were detected in the C-terminal part of the peptidomimetics (-VHLRKS) (Figure S31). These results are in accordance with the previously published crystal structure of AMPB-peptide-WDR5 complex (PDB code: 5M23) where the C-terminal part of the peptidomimetics (-VHLRKS) remained unresolved.

The binding mode of *trans* **AMPB-peptide** (**3**) remained similar to the binding mode observed in the crystallographic structure (PBD code: 5M23) (Figure S32), which further supports our computational workflow. Better stabilization of the SARA-sequence of *trans* **AMPB-peptide** (**3**) compared to the other ligands was confirmed through inspection of RMSD plots (Figure 6) and calculation standard deviations of RMSD over the 20 ns of MD simulations (Table S3). According to MD simulations of *trans* **AMPB-peptide** (**3**), valine, as the least fluctuating residue from the C-terminus of the peptidomimetic (-VHLRKS) (Figure S31), was recognized as an important residue for stabilization of the protein-ligand complex. Comparing poses of *cis* **AMPB-peptide** (**3**) and *trans* **AMPB-peptide** (**3**) (Figure 7) the N-terminal part of both peptidomimetics (SARA-) remained similar while the largest difference was in orientation of the azobenzene part of the ligand and consequently in the C-terminal part (-VHLRKS).

The binding mode of *trans* ***o*F$_4$Azo-peptide** (**5**) remained expectedly similar to *trans* **AMPB-peptide** (**3**) regarding the N-terminal domain, while the tetra-*ortho*-fluoroazobenzene moiety was partially shifted compared to the azobenzene moiety of *trans* **AMPB-peptide** (**3**) (Figure S33). The leucine within the C-terminal part (-VHLRKS), showed transient intramolecular interactions with tetra-*ortho*-fluoroazobenzene moiety during MD simulation (Figures 8A, S33 & S35). This particular intramolecular interaction was seen as the main reason for increased C-terminal valine fluctuations compared to the same valine from *trans* **AMPB-peptide (3)** during MD simulations (Figure S31). Valine retained similar binding mode inside WDR5 binding site compared to *trans* **AMPB-peptide** (**3**) (Figure S33). Nevertheless, the similar orientation and position of the C-terminal valine from the *trans* peptides **3** and **5** indicate its importance in the overall stabilization of the protein-ligand complex.

Significant shift in binding conformation of SARA- domain was observed for *cis* ***o*F$_4$Azo-peptide** (**3**) (Figure S35). Overall, the difference in observed binding modes between *cis/trans* **AMPB-peptide** (**3**) and *cis/trans* ***o*F$_4$Azo-peptide** (**5**) may be interpreted due to the different connector between SARA- domain and the novel fluorinated azobenzene. Thus, the novel peptidomimetic **5** has a 2-aminoethyl-carbamoyl linker connecting the fluorinated azobenzene and SARA- domain, instead of the methylene group of the peptidomimetic **3**, which connects the SARA-domain and unsubstituted azobenzene.

The MD calculations performed for *trans* **cAzo-peptide** (**4**) indicated that this isomer partially mimicked the positioning of other studied *trans* ligands (Figures 8C & S36). Predicted MD binding mode of *cis* **cAzo-peptide** (**4**) is comparable with its crystal structure (PDB code: 6IAM) when comparing the orientation of SARA- sequence and cyclic azobenzene moiety. This supports our computational workflow. However, some disagreement in the orientation of -VHLRKS sequence was observed (Figure S37). Interestingly, as a part of the C terminal –VHLRKS sequence, valine positioning in our crystal structure is comparable with the positioning of the isoleucine of the predicted structure, signifying the importance of this region (residues Tyr131, Phe149) of protein surface for stabilization of protein-ligand complex. Compared to *trans* **cAzo-peptide** (**4**), but also to other ligands, the C-terminal part of *cis*-**cAzo-peptide** (**4**) interacted with a smaller part of the protein binding surface,

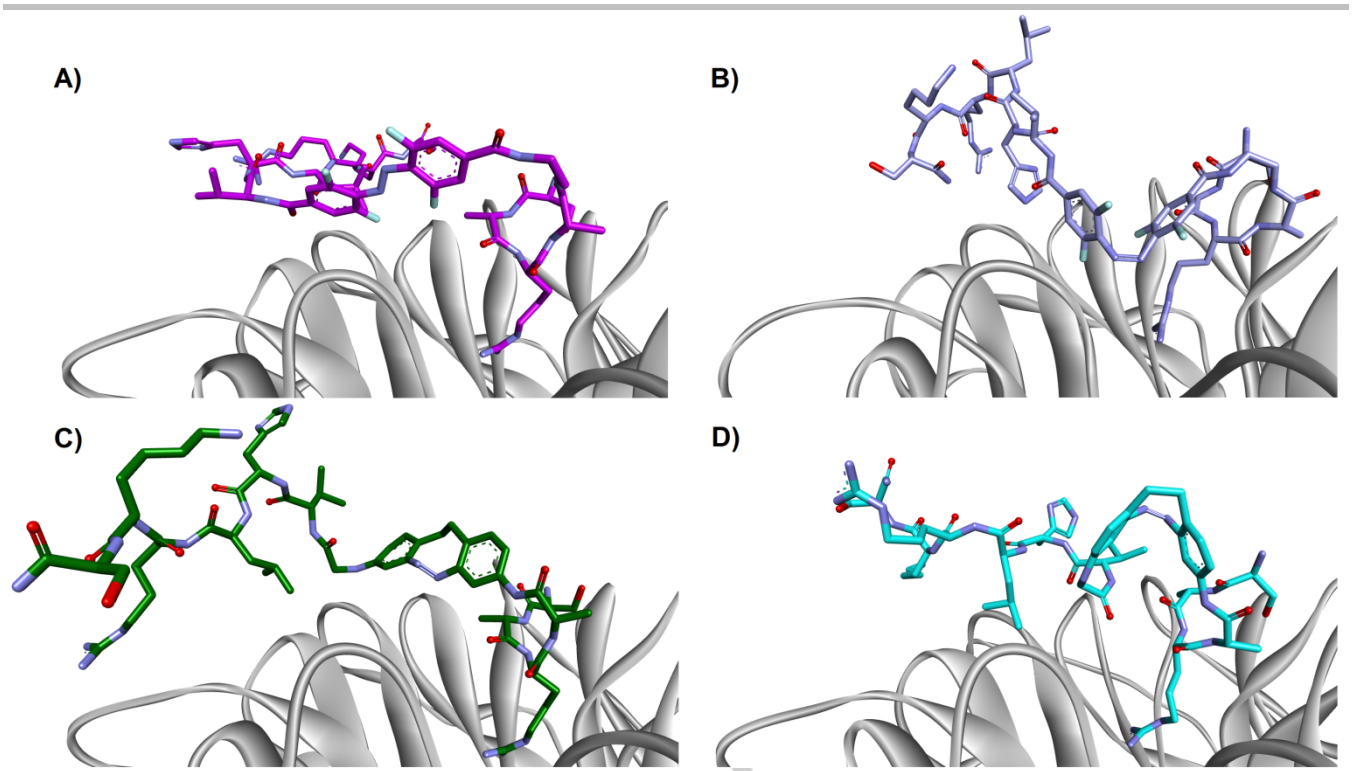

Figure 8. Binding modes of WDR5 and: A) *trans* **oF$_4$Azo-peptide** (**5**) (dark purple); B) *cis* **oF$_4$Azo-peptide** (**5**) (light purple); C) *trans* **cAzo-peptide** (**4**) (green) and D) *cis* **c-Azo peptide** (cyan).

which could be a partial explanation for the inability to crystalize protein-ligand complexes of the other peptides (Table S4).

Novel crystal structure of *cis* **cAzo-peptide** (**4**) bound to WDR5, as well as linear regression derived for experimental results (pK_i values for the synthesized peptides) and MM/PBSA scores makes this procedure promising for further *in silico* design of novel WDR5-MLL1 PPI photoswitchable disruptors. There is a need to design and synthesize novel derivatives of aforementioned peptidomimetics in order to increase the overall predictive power of such a computational study.

Table 4. Results obtained in MM/PBSA calculations and regression analysis.

Peptidomimetic	$pK_{i\,exp}$	MM/PBSA score (kJ/mol)
trans **AMPB-peptide**	8.903	-51.282
cis **AMPB-peptide**	8.187	-21.136
trans **oF$_4$Azo-peptide**	7.923	-28.388
cis **oF$_4$Azo-peptide**	7.511	-15.371
trans **cAzo-peptide**	6.854	-5.909
Cis **cAzo-petide**	6.684	-5.680

pKi_{exp} = -19.2458(MM/PBSA) + 126.4877
R^2=0.88

Conclusions

In this study, we report the synthesis of two visible-light photoswitchable amino acids to be grafted onto a peptide scaffold. The goal was to use them as visible-light responsive peptide backbone photoswitches and explore their potential as protein-protein interaction (PPI) modulators based on our former photoswitchable **AMPB-peptide**.[19] We found particularly interesting the ***o*F$_4$Azo-peptide** since the only difference with the parental compound is the *ortho*-incorporation of four fluorine atoms in the azobenzene motif and one additional methylene group in the linker of the azobenzene to the alanine. Such modification improved the photochemical characteristics of this second-generation photoswitchable PPI modulator, allowing better photoconversion under visible-light irradiation. This improvement, however, did not lead to a higher difference in the studied biological responses: neither in the WDR5 affinity nor in the MLL1 inhibition. This interesting observation highlights the difficulty to straightforward rationalize the design of effective photoswitchable PPI inhibitors and plays down the quantitative photoconversion of the molecular transducer in order to achieve functional binary system (on/off) in biological environments. For this purpose, having molecular information at our disposal is essential. Our structural activity relationships using the novel crystal structure and computational methods shed light on the binding to WDR5. Crystal structures and molecular modeling study revealed substantial difference in orientation of azobenzene

core for the characterized peptidomimetics. Agreement between experimental inhibition constant (K_i) values and results of MD turns the developed *in silico* procedure a promising tool for further design of novel closely related peptidomimetics, which is our goal for further studies.

Although quantitative photoconversion of the photoswitches might not be essential for biological applications, visible-light irradiation is an indispensable requirement for in vivo use and to avoid phototoxicity. In addition, our photocontrollable peptide backbone switches offer benefits, as fast isomerization and reversibility without degradation and high stability. Consequently, we believe that they will find applications in a wide range of light-driven molecular processes beyond protein control and related with photopharmacology, optobiology, material science, antisense chemistry or antimicrobial activity.

Experimental Section

General: All commercially reagents and solvents were purchased and used without further purification as delivered from the corresponding company (see Supporting Information for details). NMR spectra were recorded at 300 K on a Bruker AV III HD 300 MHz and 600 MHz while high resolution electrospray ionization (ESI) mass spectra were acquired with a LTQ-FT Ultra mass spectrometer (Thermo Fischer Scientific) as specified in the Supporting Information.

Peptide Synthesis: Peptides were synthesized according to the standard Fmoc-solid phase peptide methodology and purified by preparative or semipreparative HPLC. The characterization was performed via HPLC-MS and high resolution ESI. The **oF$_4$Azo-peptide** (**5**) was synthesized via a ligation reaction of the two precursor peptides: Boc-S(tBu)-A-R(Boc)$_2$-A-OH and H$_2$N-*o*F$_4$Azo-V-H(Trt)-L-R(Boc)$_2$-K(Boc)-S(tBu)-CONH$_2$.

Organic Synthesis: The precursors **6** and **9** for the photoswitchable amino acids **1** and **2** were synthesized according to literature procedures.[8-9, 32]

*Compound **7***: The compound **6** (200 mg, 0.840 mmol, 1.00 eq.) was dissolved in 4.26 mL of MeCN, under nitrogen atmosphere and DIPEA (217 mg, 1.64 mmol, 2.00 eq.) was added to this solution. After the solution was heated up to 60 °C, *tert*-butylbromoacetate (163 mg, 0.84 mmol, 1.00 eq.) was added and stirred for 15 h. Afterwards, the solvent was removed under reduced pressure and the product was isolated by flash column chromatography (pentane/EtOAc 2:1). The product **7** was obtained as a yellow solid (107 mg, 0.304 mmol, 36%). **TLC:** R_f = 0.41 (pentane/EtOAc 1:1). **^{1}H NMR** (300 MHz, $CDCl_3$, δ): 6.74 (t, ^3J = 8.2 Hz, 2H, 2 × CH_{ar}), 6.32 (dd, ^3J = 8.1 Hz, ^4J = 2.4 Hz, 1H, CH_{ar}), 6.26 (dd, ^3J = 8.2 Hz, ^4J = 2.5 Hz, 1H, CH_{ar}), 6.13 (d, ^3J = 2.4 Hz, 1H, CH_{ar}), 6.02 (d, ^3J = 2.5 Hz, 1H, CH_{ar}), 4.20 (s, 1H, NH), 3.68 (s, 2H, NHCH_2), 3.57 (s, 2H, NH_2), 2.84-2.78 (m, 2H, CH_2), 2.61-2.55 (m, 2H, CH_2), 1.46 (s, 9H, 3 × CH_3). **^{13}C NMR** (75 MHz, $CDCl_3$, δ): 170.1 (*CO*), 156.4 (*C$_{ar}$*), 156.3 (*C$_{ar}$*), 145.8 (*C$_{ar}$*), 144.9 (*C$_{ar}$*), 131.7 (*C$_{ar}$*H), 130.6 (*C$_{ar}$*H), 118.6 (*C$_{ar}$*), 117.8 (*C$_{ar}$*), 114.2 (*C$_{ar}$*H), 112.3 (*C$_{ar}$*H), 105.3 (*C$_{ar}$*H), 102.9 (*C$_{ar}$*H), 82.2 (*C*(CH$_3$)$_3$), 46.6 (CH_2NH), 31.2 (2 × CH_2), 28.2 (3 × CH_3). **HRMS-ESI+ (m/z)**: calcd. For [M+H]$^+$ $C_{20}H_{24}N_4O_2H_1$: 353.1972; found: 353.1974.

*Compound **8**:* The compound **7** (124 mg, 0.352 mmol, 1.00 eq.) dissolved in 2.30 mL of THF was cooled to 0 °C and pyridine (31.2 µL, 0.388 mmol, 1.10 eq.) was added. Then, Fmoc-Cl (100 mg, 0.288 mmol, 1.10 eq.) was added portion-wise and the mixture was stirred at r.t. for 1.5 h. The mixture was diluted with 1M HCl (2.0 mL) and was extracted with EtOAc (3 × 20.0 mL), washed with brine and dried over anhydrous $MgSO_4$. The solvent was removed in vacuo. The product **8** was isolated via flash column chromatography (pentane/EtOAc 2:1) and was obtained as a yellow solid (158 mg, 0.275 mmol, 78%). **TLC:** R_f = 0.47 (pentane/EtOAc 2:1). **^{1}H NMR** (300 MHz, $CDCl_3$, δ): 7.77 (d, ^3J = 7.8 Hz, 2H, 2 × CH_{ar}), 7.58 (d, ^3J = 7.3 Hz, 2H, 2 × CH_{ar}), 7.41 (t, ^3J = 7.3 Hz, 2H, 2 × CH_{ar}), 7.31 (td, ^3J = 7.4 Hz, ^4J = 1.0 Hz, 2H, 2 × CH_{ar}), 6.92 (d, ^3J = 8.4 Hz, 1H, CH_{ar}), 6.78 (d, ^3J = 8.2 Hz, 1H, CH_{ar}), 6.63 (m, *1H,* CH_{ar}), 6.39 (dd, ^3J = 8.3 Hz, ^4J = 2.4 Hz, 1H, CH_{ar}), 6.32 – 6.22 (m, 1H, CH_{ar}), 6.13 (d, ^3J = 2.4 Hz, 1H, CH_{ar}), 4.51 (d, ^3J = 6.4 Hz, 2H, OCH_2), 4.23 (t, ^3J = 6.4 Hz, 1H, OCH$_2$CH), 3.67 (s, 2H, NHCH_2), 3.03-2.90 (m, 2H, CH_2), 2.90-2.68 (m, 2H, CH_2), 1.44 (s, 9H, 3 × CH_3). **^{13}C NMR** (75 MHz, $CDCl_3$, δ): 168.5(*CO*), 155.8 (*CO*), 143.8 (2 x *C*$_{ar}$H), 141.4 (2 x *C*$_{ar}$H), 136.7 (2 x *C*$_{ar}$H), 130.5 (2 x *C$_{ar}$*), 128.0 (2 x *C$_{ar}$*), 127.7 (2 x *C$_{ar}$*), 127.2 (2 x *C$_{ar}$*), 127.1 (2 x *C$_{ar}$*), 125.0 (2 x *C$_{ar}$*), 124.9 (2 x *C$_{ar}$*), 120.2 (2 x *C$_{ar}$*), 120.1 (2 x *C$_{ar}$*), 82.2 (*C*CH$_3$), 68.5 (*CH$_2$*), 52.9 (*CH*), 47.2 (*CH$_2$*), 31.9 (*CH$_2$*), 31.0 (*CH$_2$*), 28.2 (3 x *CH$_3$*). **HRMS-ESI+ (m/z)**: calcd. for [M+Na]$^+$ $C_{35}H_{34}N_4O_4Na$: 597.2472; found: 597.2473.

*Compound **1**:* The compound **8** (202 mg, 0.352 mmol, 1.00 eq) was dissolved in 2.50 mL DCM and cooled to 0 °C. Then 5.00 mL TFA were added drop-wise. After stirring for 10 h at r.t., the solvent was removed under reduced pressure. The obtained residue was dissolved in EtOAc and water, extracted with EtOAc (3 × 10.0 mL) and dried over anhydrous Na_2SO_4. The solvent was removed under reduced pressure. The product was isolated by flash column chromatography (DCM/MeOH 15:1). The product **1** was obtained as a yellow solid (85.8 mg, 0.165 mmol, 47%). **TLC**: R_f = 0.06 (DCM/MeOH 15:1) **^{1}H NMR** (300 MHz, $CDCl_3$, δ): 7.74 (d, ^3J = 7.5 Hz, 2H, 2 × CH_{ar}), 7.54 (d, ^3J = 7.2 Hz, 2H, 2 × CH_{ar}), 7.38 (t, ^3J = 7.4 Hz, 2H, 2 × CH_{ar}), 7.31 – 7.21 (m, 3H, 3 × CH_{ar}), 6.82 (s, 2H, 2 × CH_{ar}), 6.71 (d, ^3J = 8.3 Hz, 1H, CH_{ar}), 6.21 (dd, ^3J = 8.2 Hz, ^4J = 2.4 Hz, 1H, CH_{ar}), 5.96 (t, ^3J = 4.2 Hz, 1H, CH_{ar}), 4.48 (d, ^3J = 6.4 Hz, 2H, OCH_2), 4.20 (d, ^3J = 6.4 Hz, 1H, OCH$_2$CH), 3.74 (s, 2H, NHCH_2), 2.91 – 2.79 (m, 2H, CH_2), 2.67 – 2.54 (m, 12H, CH_2). **^{13}C NMR** (75 MHz, $CDCl_3$, δ): 174.3 (*CO*), 156.2 (*CO*), 155.8 (2 × *C$_{ar}$*), 145.6 (2 × *C$_{ar}$*), 143.7 (2 × *C$_{ar}$*), 141.5 (2 × *C$_{ar}$*), 136.1 (*C$_{ar}$*), 130.8 (2 × *C$_{ar}$*H), 130.4 (2 × *C$_{ar}$*H), 128.0 (2 × *C$_{ar}$*H), 127.3 (2 × *C$_{ar}$*H), 125.0 (2 × *C$_{ar}$*H), 120.2 (2 × *C$_{ar}$*H), 118.2 (*C$_{ar}$*), 112.7 (*C$_{ar}$*H), 102.8 (*C$_{ar}$*H), 67.1 (CHCH$_2$), 47.2 (*C*HCH$_2$), 45.8 (NHCH$_2$), 31.3 (*CH$_2$*), 30.9 (*CH$_2$*). **HRMS-ESI+ (m/z)**: calcd. for [M+H]$^+$: $C_{31}H_{26}N_4O_4H_1$: 519.2038; found: 519.2019.

*Compound **2**:* The compound **9** (275. mg, 0.804 mmol, 1.50 eq.) was suspended in THF (20.0 mL). HATU (206 mg, 0.536 mmol, 1.00 eq.) and DIPEA (187 µL, 1.61 mmol, 2.00 eq.) were added and the resulting solution was stirred at r.t. After 15 min the N1-(diphenyl(p-tolyl)methyl)ethane-1,2-diamine (**10**, 210 mg, 0.665 mmol, 1.20 eq) in THF (7.00 mL) was added and the solution was stirred for 3 h at rt. Afterwards the solvent was removed under reduced pressure and the crude was purified by flash column chromatography (DCM:MeOH 45:1 + 3% NEt$_3$) to yield the desired product **2** as the triethylamine salt (244 mg, 0.329 mmol, 61%) red solid. To obtain the NMR spectra without the triethylamine traces, a small amount was further purified by flash column chromatography (DCM:MeOH 45:1 + 3% NH$_3$). **TLC:** R_f = 0.16 (DCM:MeOH 45:1 + 3% NEt$_3$). **^{1}H NMR** (300 MHz, DMSO, δ): 8.87 (s, 1H, CON*H*CH$_2$), 7.80 (d, ^3J = 10.6 Hz, 4H, 4 × CH_{ar}), 7.42 (d, ^3J = 7.4 Hz, 4H, 4 × CH_{ar}), 7.28 (t, ^3J = 6.7 Hz, 6H, 6 × CH_{ar}), 7.20 (d, ^3J = 7.1 Hz, 2H, 2 × CH_{ar}), 7.09 (d, ^3J = 8.0 Hz, 2H, 2 × CH_{ar}), 3.48-3.46 (m, 2H CH_2NH), 2.26 (s, 3H CH_3), 2.16 (m, 2H CH_2NH). **^{13}C NMR** (75 MHz, DMSO, δ): 164.5 (*CO*), 162.8 (*CO*), 156.1 (*C$_{ar}$*F), 155.9 (*C$_{ar}$*F), 152.6 (*C$_{ar}$*F), 152.4 (*C$_{ar}$*F), 150.3 (*C$_{ar}$*C), 146.1 (2 × *C$_{ar}$*C), 144.0 (*C$_{ar}$*C), 142.9 (*C$_{ar}$*C), 138.7 (*C$_{ar}$*C), 135.7 (*C$_{ar}$*C), 135.0 (*C$_{ar}$*C), 128.3 (4 × *C$_{ar}$*H), 128.2 (2 × *C$_{ar}$*H), 127.6 (4 × *C$_{ar}$*H), 127.5 (2 × *C$_{ar}$*H), 125.9 (2 × *C$_{ar}$*H), 113.9 (*C$_{ar}$*HCF), 113.6 (*C$_{ar}$*HCF), 112.2 (*C$_{ar}$*HCF), 111.9 (*C$_{ar}$*HCF), 82.4 (NHC*C*$_4$), 70.1 (NH*C*H$_2$), 43.1 (NH*C*H$_2$), 20.4 (*CH$_3$*).

HRMS-ESI+ (m/z): calcd. for $[M-H]^-$ $C_{36}H_{27}F_4N_4O_3$, 639.2025; found: 639.2025.

UV-Vis Spectroscopy and Fluorescence Polarization Measurements: Concentration determinations, UV-vis and fluorescence polarization based measurements were performed on a Tecan (Switzerland) Spark 20M multimode microplate reader at room temperature. All measurements for concentration determinations were performed in a 1400 µL quartz cuvette (Hellma Analytics (104F-QS) with a pathlength of 1 cm. Fluorescence polarization assays were performed as described previously[19] in black 96-well microtiter plates (Greiner, ref. nr.: 655900) with excitation at 485 nm and emission at 530 nm. The detailed procedure of the fluorescence polarization-based assays is in the Supporting Information. K_i values were calculated following the equation described previously by Wang et al. and the corresponding webpage provided by them.[28]

AlphaLISA HMT Assay: The AlphaLISA HMT assay was performed in white 384 well plates (Corning, ref. nr.: 4512) and with the AlphaLISA buffer (50 mM Tris pH 8.0, 50 mM NaCl, 5 mM $MgSO_4$, 10% glycerol, 0.01% Tween-20, 1 mM DTT). The MLL1 complex (MLL1, WDR5Δ23, Ash2L, RBbP5) was reconstituted in the AlphaLISA buffer to obtain a 205 nM solution. Each reaction contained final concentrations of 100 nM of MLL1 complex, 1.70 µM of the substrate H_3-21mer peptide (Anaspec) and 2.00 µM of the cofactor S-adenosylmethionine (SAM, Perkin Elmer). Both, the *trans* and the *cis* isomers of the peptidomimetic **5** (*trans*: previously irradiated at 405 nm for 5 min; *cis*: previously irradiated at 520 nm for 5 min, as explained in the Supporting Information) were added at concentrations ranging from 1.70 nM to 150.0 µM and incubated with the pre-assembled MLL1 complex for 20 min on ice. Each plate contained triplicates of a negative DMSO biograde control, a positive control with the already methylated H_3-peptide and a blank with just buffer and DMSO. Reactions were initiated by addition of the H3/SAM mixture and incubated for 3 h at room temperature, before the acceptor and donor Alpha-beads (equilibrated with the AlphaLISA buffers) were added. After other 2 h of incubation at r.t., luminescence was measured on a Perkin Elmer EnVision plate reader (mirror: 444, emission: 570 nm. The experiment was performed in triplicate three times, independently.

GST-Pull Down Assay: For the GST-pull down assay 500 µL of GST tagged MLL1 in assay buffer (50 mM Tris, 150 mM NaCl, 1.00 mM PMSF, protease inhibitor) with 0.05% NP-40 and 1 × BSA were preincubated on a rotator with 20.0 µL of glutathione-sepharose beads (equilibrated with assay buffer) with a final concentration of 0.262 µM for 1.5 h at 4°C. After three washing steps of the beads with lysis buffer (assay buffer + 0.5% NP-40), the remaining proteins (WDR5Δ23, Ash2L, RbBP5) in assay buffer with 0.05% NP-40 and 1 × BSA were added to the beads with a final concentration of 0.4 µM. After incubating 5 min on ice, the respective concentrations (200 µM, 30 µM, 5 µM) of the peptidomimetic **5** in DMSO (*cis* and *trans*: photoisomerization done as explained in the Supporting Information) were added and the mixture was incubated on the rotator at 4 °C for 3 h. A negative control, where no GST-MLL1 was added, as well as a positive DMSO biograde control were included in each assay. After 3 h, the beads were washed 5 × with lysis buffer, incubated with 80 µL SDS-loading dye (0.5 M Tris pH = 6.8), 5% SDS, 25% glycerol, 5% bromphenol blue in MilliQ water) and the proteins were denatured by incubation at 95 °C for 5 min. After running a SDS-PAGE (12%, followed protocol of the *Lab FAQs* from Roche) the bound proteins were detected via immunoblots (Western-Blot buffers followed protocol of the *Lab FAQs* from Roche and procedure followed *Western Blotting Protocol* (Tank Transfer) from Sigma Aldrich) using the appropriate antibodies (rabbit-antibodies from Bethyl, USA: anti-MLL1 (A300-375A), anti-WDR5 (A302-429A), anti-RbBP5 (A300-109A)).

Crystallization, Data Collection, Structure Determination and Analysis:

*Crystallisation of WDR5Δ23-Peptide **4** Complex*: WDR5 was concentrated to 200 µM, mixed with 25.9 mM of the cAzo-containing peptide **4** to yield final concentrations of 194 µM protein and 792.5 µM **4** (ratio: 1:4 protein/peptide) and crystallized in SWISSCI MRC two-well crystallization plates (Jena Bioscience). The reservoir solution volume was 50 µL, the drops contained 1 µL of a 1:1 mixture of protein and crystallisation solution. Crystal growth took place at 4°C in a solution containing 10% (w/v) PEG 20 000, 20% (v/v) PEG 550 MME, 0.02 M sodium formate, 0.02 M ammonium acetate, 0.02 M trisodium citrate, 0.02 M sodium potassium L-tartrate and 0.02 M sodium oxamate. Crystals were obtained after 2 weeks and flash-cooled in liquid nitrogen without additional cryoprotectant. Diffraction data were collected at the European Synchrotron Radiation Facility (ESRF) using beamline ID23-2 equipped with a microdiffractometer and Pilatus3 x 2M detector. The crystals diffracted to 1.51 Å using X-ray radiation of 14.2 keV (0.873 Å). The data were processed using XDS[33] in Space Group P 1 21 1. Data reduction and scaling were done using CCP4i2 (Version 7.0.065),[34] using AIMLESS (Version 0.7.3).[35] The phases were solved by molecular replacement with the previously determined structure of the WDR5 in complex with another peptidomimetic inhibitor (PDB code: 5M23)[19] using PHASER.[36] The model was built using COOT (Version 0.8.9).[37] and refinement in PHENIX (Version 1.11.1)[38] until a R_{work} of 16.7% and a R_{free} of 17.2% were achieved. The peptidomimetic restraints were generated via ReadySet.[38] Final refinement statistics are given in Table 3. All structural representation were generated using PyMOL (Version 2.2). The coordinates and structure factors have been deposited to the Protein Data Bank under PDB code 6IAM.

Molecular Docking: For virtual docking of ligands into WDR5, GOLD 5.6 software[39] was used. Docking of peptides as PPI inhibitors still represent challenging task due to significant flexibility of peptides and challenges in identifications of hot-spot regions on protein surfaces.[40] Although, there are spatialized algorithms for docking of peptides, GOLD algorithm, primarily intended for small-molecules docking, has been proven to be accurate and fast alternative,[41] especially in this particular case where it was reasonable to assume that ARA sequence retain similar binding mode. Application of the more specialized methodologies for peptide-protein docking was hampered by the fact that photoswitch in our ligands was introduced in the middle of peptide sequence, making them unsuitable for those procedures. Exploiting the known SARA- sequence conformation obtained in PDB code: 5M23, docking procedure in GOLD was set in two steps in which fragment-based approach for molecular docking was employed. Docking protocol was set up in two steps: **1)** Fragment SARA–Azo (where Azo indicates azobenzenes/diazocines) was docked in PDB code: 5M23 using substructure constrains on SARA- sequence. SARA-sequence conformation was retained from PDB, while Azo was manually added to the SARA- sequence and final conformation for first docking was generated in 20 ns MD run of this ligand with position restrains added to SARA- sequence using Gromacs 5.1.4 software, as it's explained in next section (Molecular Dynamics). **2)** Docking of whole molecule was performed by constraining SARA-Az- pose obtained in previous docking step. Peptide fragment (-VHLRKS sequence) was built in DS Visualizer in β-sheet conformation. Final confirmation of ligand VHLRKS sequence was generated after 20 ns MD run of ligand with position restrains added to SARA- sequence, using Gromacs 5.1.4 software as it is explained in next section (Molecular Dynamics). For molecular docking, PLP scoring function was used, with 50 poses generated and maximum flexibility accounted for ligands. Binding site was selected as the area of 8Å around ligand. Constraint weights were 20 for SARA- sequence and 5 for azobenzene. Only poses with smallest RMSD of SARA- sequence

compared to PDB code: 5M23 were retained for further molecular dynamics study.

Molecular Dynamics (MD): MD protocol included definition of azobenzenes as novel residues. Parameters for azobenzenes have been obtained from ParamChem web-server[42] and manually included in Charmm36 force-field.[43]. GROMACS 5.1.4 software was used for all MD simulations. The protonation for protein-ligand complexes were determined with PROPKA server.[44] The protein was parametrized by CHARMM36 force field, whereas the amino-acids of the ligands. The water model employed was TIP3P, and the octahedron simulation box has been used. The solvated system was preliminary minimized by 5000 steps of steepest descent. The system was then heated to 310K during 250 ps in NVT ensemble with 1 fs time step. After that, the pressure was equilibrated to 1 atm during 500 ps NPT simulation with 2 fs time step. In the equilibration steps harmonic positional restraints were set on the backbone of the protein with a spring constant of 1000 kJ/(mol·Å^2). The position restraints used in equilibration were gradually removed during 1 ns simulation with 2 fs time step. The production run was carried out in the NPT ensemble at 310 K without any restraint, except for simulations with ligands only where position restrains were kept on –SARA- sequence. The Verlet cutoff scheme, the Nose−Hoover thermostat, Parrinello–Rahman barostat, LINCS for the constraints (all bonds with H atoms), and the particle mesh Ewald for electrostatics were applied. Upon completion of the simulation, a Gromos clustering process[45] on the molecular dynamics trajectory and relevant cluster representatives were obtained. MD simulations were used for refinement of complexes generated by molecular docking. Only simulations where ARA sequence was maintained stabile in active site have been retained for further MM/PBSA analysis.

MM/PBSA Scoring: Molecular Mechanics/Poisson-Boltzmann Surface Area (MM/PBSA) method was used for post-processing of data generated form molecular dynamics simulations. This method, as an end point free energy calculation methodology, has been proven as a useful tool for post-processing results obtained by molecular docking followed with MD refinement.[46] Although, this method is not accurate enough for prediction of absolute binding free energies, mostly because MM/PBSA counts on severe thermodynamic approximations, it has been proven useful for rationalization of experimental results on series of similar ligands by ranking relative binding affinities.[46-47] Here, we used 20 ns production MD runs for refinement of obtained docking poses, and GMXPBSA 2.1 tool for calculation of binding energies from every 18th snapshots extracted in last 7 ns of simulations (total of 21 snapshots per trajectory) with single-trajectory approach. Dielectric constant of solute was switched to 1, while all other parameters were retained on default values. The entopic term was neglected from calculation.

Acknowledgements

The authors gratefully acknowledge: Prof. Dr. E. Meggers for S1 laboratory accessibility; N. Frommknecht for design assistance and construction of the LED lamps. Numerical simulations were run on the PARADOX-IV supercomputing facility at the Scientific Computing Laboratory, National Center of Excellence for the Study of Complex Systems, Institute of Physics Belgrade, supported in part by the Ministry of Education, Science, and Technological Development of the Republic of Serbia under project No. ON171017. NDj, DR and KN acknowledge project of Ministry of Science and Technological Development of the Republic of Serbia No 172033. Finally, we thank COST action CM1406 (Epigenetic Chemical Biology EPICHEMBIO) for support.

Keywords: protein-protein interactions • photoswitches • azobenzene • photopharmacology • visible-light irradiation

[1] a) L. Bonetta, *Nature* **2010**, *468*, 851-854; b) H. C. Lu, A. Fornili, F. Fraternali, *Expert. Rev. Proteomics* **2013**, *10*, 511-520.

[2] a) D. E. Scott, A. R. Bayly, C. Abell, J. Skidmore, *Nat. Rev. Drug Discov.* **2016**, *15*, 533-550; b) S. Surade, T. L. Blundell, *Chem. Biol.* **2012**, *19*, 42-50.

[3] a) N. Sawyer, A. M. Watkins, P. S. Arora, *Acc. Chem. Res.* **2017**, *50*, 1313-1322; b) I. S. Moreira, O. Sensoy, *Curr. Top Med. Chem.* **2018**, *18*, 645-646; c) T. Berg, *Angew. Chem. Int. Ed. Engl.* **2003**, *42*, 2462-2481; d) S. Gul, K. Hadian, *Expert. Opin. Drug Discov.* **2014**, *9*, 1393-1404; e) L. G. Milroy, T. N. Grossmann, S. Hennig, L. Brunsveld, C. Ottmann, *Chem. Rev.* **2014**, *114*, 4695-4748; f) J. A. Wells, C. L. McClendon, *Nature* **2007**, *450*, 1001-1009; g) D. C. Fry, *Methods Mol. Biol.* **2015**, *1278*, 93-106; h) L. C. Cesa, A. K. Mapp, J. E. Gestwicki, *Front. Bioeng. Biotechnol.* **2015**, *3*, 119.

[4] a) L. Nevola, E. Giralt, *Chem. Commun. (Camb)* **2015**, *51*, 3302-3315; b) M. Pelay-Gimeno, A. Glas, O. Koch, T. N. Grossmann, *Angew. Chem. Int. Ed. Engl.* **2015**, *54*, 8896-8927; c) A. Barnard, K. Long, H. L. Martin, J. A. Miles, T. A. Edwards, D. C. Tomlinson, A. Macdonald, A. J. Wilson, *Angew. Chem. Int. Ed. Engl.* **2015**, *54*, 2960-2965; d) P. Wojcik, L. Berlicki, *Bioorg. Med. Chem. Lett.* **2016**, *26*, 707-713.

[5] a) R. J. Mart, R. K. Allemann, *Chem. Commun.* **2016**, *52*, 12262-12277; b) H. M. D. Bandara, S. C. Burdette, *Chem. Soc. Rev.* **2012**, *41*, 1809-1825.

[6] a) M. M. Lerch, M. J. Hansen, G. M. van Dam, W. Szymanski, B. L. Feringa, *Angew. Chem. Int. Ed. Engl.* **2016**, *55*, 10978-10999; b) J. Broichhagen, J. A. Frank, D. Trauner, *Accounts Chem. Res.* **2015**, *48*, 1947-1960; c) Z. B. Mehta, N. R. Johnston, M. S. Nguyen-Tu, J. Broichhagen, P. Schultz, D. P. Larner, I. Leclerc, D. Trauner, G. A. Rutter, D. J. Hodson, *Sci. Rep.-Uk* **2017**, *7*; d) A. A. Beharry, G. A. Woolley, *Chem. Soc. Rev.* **2011**, *40*, 4422-4437.

[7] a) M. X. Dong, A. Babalhavaeji, S. Samanta, A. A. Beharry, G. A. Woolley, *Accounts Chem. Res.* **2015**, *48*, 2662-2670; b) H. A. Wegner, *Angew. Chem. Int. Ed. Engl.* **2012**, *51*, 4787-4788; c) C. Knie, M. Utecht, F. L. Zhao, H. Kulla, S. Kovalenko, A. M. Brouwer, P. Saalfrank, S. Hecht, D. Bleger, *Chem.-Eur. J.* **2014**, *20*, 16492-16501; d) M. Wegener, M. J. Hansen, A. J. M. Driessen, W. Szymanski, B. Feringa, *J. Am. Chem. Soc.* **2017**, *139*, 17979-17986; e) Z. Pianowski, *Chemistry* **2019,** *in press doi: 10.1002/chem.201805814*.

[8] R. Siewertsen, H. Neumann, B. Buchheim-Stehn, R. Herges, C. Nather, F. Renth, F. Temps, *J. Am. Chem. Soc.* **2009**, *131*, 15594-15595.

[9] a) H. Sell, C. Nather, R. Herges, *Beilstein J. Org. Chem.* **2013**, *9*, 1-7; b) S. Samanta, C. Qin, A. J. Lough, G. A. Woolley, *Angew. Chem. Int. Ed. Engl.* **2012**, *51*, 6452-6455.

[10] A. A. Beharry, O. Sadovski, G. A. Woolley, *J. Am. Chem. Soc.* **2011**, *133*, 19684-19687.

[11] a) M. Cigl, A. Bubnov, M. Kaspar, F. Hampl, V. Hamplova, O. Pacherova, J. Svoboda, *J. Mater. Chem. C* **2016**, *4*, 5326-5333; b) J. Karcher, Z. L. Pianowski, *Chemistry* **2018**, *24*, 11605-11610.

[12] J. Luo, S. Samanta, M. Convertino, N. V. Dokholyan, A. Deiters, *Chembiochem* **2018**, *19*, 2178-2185.

[13] F. Eljabu, J. Dhruval, H. B. Yan, *Bioorganic Med. Chem. Lett.* **2015**, *25*, 5594-5596.

[14] D. C. Burns, F. Zhang, G. A. Woolley, *Nat. Protoc.* **2007**, *2*, 251-258.

[15] a) M. Bose, D. Groff, J. M. Xie, E. Brustad, P. G. Schultz, *J. Am. Chem. Soc.* **2006**, *128*, 388-389; b) A. A. John, C. P. Ramil, Y. L. Tian, G. Cheng, Q. Lin, *Org. Lett.* **2015**, *17*, 6258-6261.

[16] R. Behrendt, M. Schenk, H. J. Musiol, L. Moroder, *J. Pept. Sci.* **1999**, *5*, 519-529.

[17] L. Ulysse, J. Chmielewski, *Bioorganic Med. Chem. Lett.* **1994**, *4*, 2145-2146.

[18] D. Bleger, J. Schwarz, A. M. Brouwer, S. Hecht, *J. Am. Chem. Soc.* **2012**, *134*, 20597-20600.

[19] L. Albert, J. Xu, R. W. Wan, V. Srinivasan, Y. L. Dou, O. Vazquez, *Chem. Sci.* **2017**, *8*, 4612-4618.

[20] a) Z. Ahmed, A. Siiskonen, M. Virkki, A. Priimagi, *Chem. Commun.* **2017**, *53*, 12520-12523; b) M. D. Wendt, A. R. Kunzer, *Tetrahedron Lett.* **2010**, *51*, 641-644.

[21] B. Sax, F. Dick, R. Tanner, J. Gosteli, *Peptide Res.* **1992**, *5*, 245-246.
[22] D. Chouikhi, M. Ciobanu, C. Zambaldo, V. Duplan, S. Barluenga, N. Winssinger, *Chemistry* **2012**, *18*, 12698-12704.
[23] K. Ralhan, V. G. KrishnaKumar, S. Gupta, *Rsc Adv.* **2015**, *5*, 104417-104425.
[24] G. B. Fields, *Methods Mol. Biol.* **1994**, *35*, 17-27.
[25] S. Z. Li, G. Han, W. Q. Zhang, *Macromolecules* **2018**, *51*, 4290-4297.
[26] a) H. R. Lopez-Mirabal, J. R. Winther, *Biochim. Biophys. Acta* **2008**, *1783*, 629-640; b) C. Boulegue, M. Loweneck, C. Renner, L. Moroder, *Chembiochem* **2007**, *8*, 591-594.
[27] Y. Dou, T. A. Milne, A. J. Ruthenburg, S. Lee, J. W. Lee, G. L. Verdine, C. D. Allis, R. G. Roeder, *Nat. Struct. Mol. Biol.* **2006**, *13*, 713-719.
[28] Z. Nikolovska-Coleska, R. Wang, X. Fang, H. Pan, Y. Tomita, P. Li, P. P. Roller, K. Krajewski, N. G. Saito, J. A. Stuckey, S. Wang, *Anal. Biochem.* **2004**, *332*, 261-273.
[29] H. Karatas, Y. Li, L. Liu, J. Ji, S. Lee, Y. Chen, J. Yang, L. Huang, D. Bernard, J. Xu, E. C. Townsend, F. Cao, X. Ran, X. Li, B. Wen, D. Sun, J. A. Stuckey, M. Lei, Y. Dou, S. Wang, *J. Med. Chem.* **2017**, *60*, 4818-4839.
[30] A. J. Ruthenburg, W. Wang, D. M. Graybosch, H. Li, C. D. Allis, D. J. Patel, G. L. Verdine, *Nat. Struct. Mol. Biol.* **2006**, *13*, 704-712.
[31] a) N. L. Alicea-Velazquez, S. A. Shinsky, D. M. Loh, J. H. Lee, D. G. Skalnik, M. S. Cosgrove, *J. Biol. Chem.* **2016**, *291*, 22357-22372; b) J. J. Song, R. E. Kingston, *J. Biol. Chem.* **2008**, *283*, 35258-35264; c) A. Patel, V. Dharmarajan, M. S. Cosgrove, *J. Biol. Chem.* **2008**, *283*, 32158-32161.
[32] D. Bleger, S. Hecht, *Angew. Chem. Int. Ed. Engl.* **2015**, *54*, 11338-11349.
[33] W. Kabsch, *Acta Crystallogr. D Bio.l Crystallogr.* **2010**, *66*, 125-132.
[34] M. D. Winn, C. C. Ballard, K. D. Cowtan, E. J. Dodson, P. Emsley, P. R. Evans, R. M. Keegan, E. B. Krissinel, A. G. Leslie, A. McCoy, S. J. McNicholas, G. N. Murshudov, N. S. Pannu, E. A. Potterton, H. R. Powell, R. J. Read, A. Vagin, K. S. Wilson, *Acta Crystallogr. D Biol- Crystallogr.* **2011**, *67*, 235-242.
[35] P. R. Evans, G. N. Murshudov, *Acta Crystallogr. D Biol. Crystallogr.* **2013**, *69*, 1204-1214.
[36] A. J. McCoy, R. W. Grosse-Kunstleve, P. D. Adams, M. D. Winn, L. C. Storoni, R. J. Read, *J. Appl. Crystallogr.* **2007**, *40*, 658-674.
[37] P. Emsley, B. Lohkamp, W. G. Scott, K. Cowtan, *Acta Crystallogr. D Biol. Crystallogr.* **2010**, *66*, 486-501.
[38] P. D. Adams, P. V. Afonine, G. Bunkoczi, V. B. Chen, I. W. Davis, N. Echols, J. J. Headd, L. W. Hung, G. J. Kapral, R. W. Grosse-Kunstleve, A. J. McCoy, N. W. Moriarty, R. Oeffner, R. J. Read, D. C. Richardson, J. S. Richardson, T. C. Terwilliger, P. H. Zwart, *Acta Crystallogr. D Biol. Crystallogr.* **2010**, *66*, 213-221.
[39] G. Jones, P. Willett, R. C. Glen, A. R. Leach, R. Taylor, *J. Mol. Biol.* **1997**, *267*, 727-748.
[40] M. Ciemny, M. Kurcinski, K. Kamel, A. Kolinski, N. Alam, O. Schueler-Furman, S. Kmiecik, *Drug Discov. Today* **2018**, *23*, 1530-1537.
[41] a) A. S. Hauser, B. Windshugel, *J Chem Inf Model* **2016**, *56*, 188-200; b) C. Lammi, C. Zanoni, G. Aiello, A. Arnoldi, G. Grazioso, *Sci. Rep.* **2016**, *6*, 29931.
[42] K. Vanommeslaeghe, E. Hatcher, C. Acharya, S. Kundu, S. Zhong, J. Shim, E. Darian, O. Guvench, P. Lopes, I. Vorobyov, A. D. Mackerell, Jr., *J Comput. Chem.* **2010**, *31*, 671-690.
[43] J. Huang, A. D. MacKerell, Jr., *J Comput. Chem.* **2013**, *34*, 2135-2145.
[44] M. H. Olsson, C. R. Sondergaard, M. Rostkowski, J. H. Jensen, *J Chem Theory Comput.* **2011**, *7*, 525-537.
[45] X. Daura, K. Gademann, B. Jaun, D. Seebach, W. F. van Gunsteren, A. E. Mark, *Angew. Chem. Int. Edit.* **1999**, *38*, 236-240.
[46] T. Hou, J. Wang, Y. Li, W. Wang, *J. Chem. Inf. Model* **2011**, *51*, 69-82.
[47] a) H. Y. Sun, Y. Y. Li, M. Y. Shen, S. Tian, L. Xu, P. C. Pan, Y. Guan, T. J. Hou, *Phys. Chem. Chem. Phys.* **2014**, *16*, 22035-22045; b) S. Genheden, U. Ryde, *Expert. Opin. Drug Discov.* **2015**, *10*, 449-461.

Entry for the Table of Contents (Please choose one layout)

Layout 1:

FULL PAPER

Bright shot! Optic control of enzymatic activity by using visible-light photoswitchable protein-protein modulators.

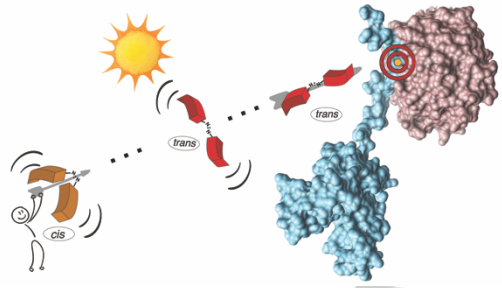

*Lea Albert, Alberto Peñalver, Nemanja Djokovic, Laura Werel, Malte Hoffarth, Dusan Ruzic, Jing Xu, Lars-Oliver Essen, Katarina Nikolić, Yali Dou, Olalla Vázquez**

Page No. – Page No.

Modulating Protein-Protein Interactions with Visible-Light Responsive Peptide Backbone Photoswitches